

Charge Transfer and Zhang-Rice singlet bands in the Nickelate Superconductor $\text{La}_3\text{Ni}_2\text{O}_7$ under Pressure

Wéi Wú,^{1,*} Zhihui Luo,¹ Dao-Xin Yao,¹ and Meng Wang¹

¹Center for Neutron Science and Technology, Guangdong Provincial Key Laboratory of Magnetoelectric Physics and Devices, School of Physics, Sun Yat-sen University, Guangzhou, Guangdong 510275, China

(Dated: October 9, 2023)

Recently, a bulk nickelate superconductor $\text{La}_3\text{Ni}_2\text{O}_7$ is discovered at pressures with a remarkable high transition temperature $T_c \sim 80\text{K}$. Here, we study a Hubbard model with tight-binding parameters derived from *ab initio* calculations of $\text{La}_3\text{Ni}_2\text{O}_7$, by employing large scale determinant quantum Monte Carlo and cellular dynamical mean-field theory. Our result suggests that the superexchange couplings in this system are comparable to that of cuprates. The system is a charge transfer insulator as hole concentration becomes four per site at large Hubbard U . Upon hole doping, two low-energy spin-singlet bands emerge in the system exhibiting distinct correlation properties: while the one composed of the out-of-plane Ni- $d_{3z^2-r^2}$ and O- p_z orbitals demonstrates strong antiferromagnetic correlations and narrow effective bandwidth, the in-plane singlet band consisting of the Ni- $d_{x^2-y^2}$ and O- p_x/p_y orbitals is in general more itinerant. Over a broad range of hole doping, the doped holes occupy primarily the $d_{x^2-y^2}$ and p_x/p_y orbitals, whereas the $d_{3z^2-r^2}$ and p_z orbitals remain underdoped. We propose an effective $t - J$ model to capture the relevant physics and discuss the implications of our result for comprehending the $\text{La}_3\text{Ni}_2\text{O}_7$ superconductivity.

INTRODUCTION

Since the discovery of cuprate superconductors [1], understanding and searching for novel high transition temperature (high- T_c) superconductors [2–17] has been one of the major focuses in the condensed matter physics. The discovery of infinite layer nickelate superconductor [18–31] marks a notable recent advancement, although in which the superconductivity (SC) has been only observed in thin films on substrates [18], but not yet in bulk samples [32]. The very recently discovered bulk superconductor $\text{La}_3\text{Ni}_2\text{O}_7$ under high pressures [2], which exhibits a remarkable T_c of ~ 80 Kelvins, then represents a significant breakthrough in this field. As revealed by the density-functional theory (DFT) calculations [2, 3, 33], a hallmark of the nickelate bi-layer $\text{La}_3\text{Ni}_2\text{O}_7$ [2, 34] is the activating of both $3d_{x^2-y^2}$ and $3d_{3z^2-r^2}$ orbitals in vicinity of Fermi level [3, 35]. This distinct feature may lead to superconductivity that differs significantly from the cuprates and infinite layer nickelates. From a theoretical perspective, several crucial questions arise. First, to understand the driving force behind the SC, it is necessary to elucidate the magnetic exchange couplings [23, 36] among the four active e_g orbitals in the NiO_2 bi-layer. Moreover, the e_g orbitals of $\text{La}_3\text{Ni}_2\text{O}_7$ under pressure possess a large hole content, as the nominal valence of Ni is $\text{Ni}^{2.5+}$ in this system, indicating an average of 1.25 holes per e_g orbital. This high hole concentration level is on the verge of quenching SC by overdoping in the context of cuprates. Therefore, resolving the distributions of the holes in the Ni- e_g orbitals and the correlated O- $2p$ orbitals is crucial for understanding the correlation effects in $\text{La}_3\text{Ni}_2\text{O}_7$ under pressure [37].

To address above questions, here we study an 11-band Hubbard model that includes four $3d_{x^2-y^2}$ /

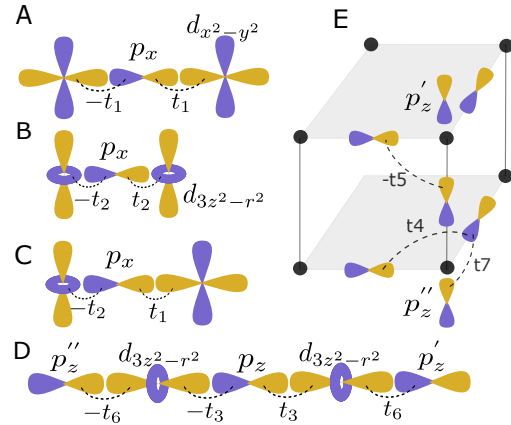


FIG. 1. (Color online) The seven hopping terms in our 11-band Hubbard model [3]. **A-D**: Four hopping processes between Ni- d and O- p orbitals that lead to major superexchanges between Ni- d orbitals. Here $t_1 = -1.56$, $t_2 = 0.75$, $t_3 = -1.63$, $t_6 = 1.37$. The site energy $\epsilon_{d_{x^2-y^2}} = -1.06$, $\epsilon_{d_{3z^2-r^2}} = -1.16$, $\epsilon_{p_x/p_y} = -4.94$, $\epsilon_{p_z} = -4.30$, $\epsilon_{p_z''} = \epsilon_{p_z'} = -3.77$. Note that the hopping process (C) is from combining A and B. The superexchange between the on-site intra-layer $d_{x^2-y^2}$ and $d_{3z^2-r^2}$ orbitals (not shown here) vanishes due to symmetry. **E**: Hoppings between O- p orbitals are shown on a cartoon depicting the structure of the bilayer NiO_2 planes. The $3d$ orbitals in Ni (black dots) are not shown for clarity. Here $t_4 = 0.58$, $t_5 = 0.49$, $t_7 = 0.43$. These seven hopping terms combining the site-energies define our 11-band Hubbard model in the non-interacting limit.

$3d_{3z^2-r^2}$ orbitals of nickel, and seven most relevant $2p$ orbitals of oxygen in the NiO_2 bi-layer per site. We carry out determinant quantum Monte Carlo simulations (DQMC) [38, 39] and cellular dynamical mean-field theory (CDMFT) [40, 41] calculations in the normal state of the system. Our result suggests that the superexchange

couplings in this system are in general comparable to that in cuprates [42], supporting a magnetic correlation origin of the high T_c superconductivity in $\text{La}_3\text{Ni}_2\text{O}_7$ under pressure. We show that at large Hubbard U , the system is a charge-transfer insulator [43] in the Zaanen-Sawatzky-Allen (ZSA) scheme [44] at half-filling (*i.e.*, four holes per site). Upon hole doping, the vertical Ni- $d_{3z^2-r^2}$ - O- p_z orbitals host a narrow low-energy spin-singlet band, where a small doping level is maintained over a broad range of hole doping of the system. In contrast, the in-plane Ni- $d_{x^2-y^2}$ and O- p_x/p_y orbitals form low-energy singlet band with high propensity for hole doping and greater itinerancy, drawing an analogy to the Zhang-Rice singlet band (ZRSB) in cuprates [45–47]. We discuss the implication of this inhomogeneous distribution of holes in the two e_g orbitals to the superconductivity. An effective t - J model that considers the leading-order exchange couplings in $\text{La}_3\text{Ni}_2\text{O}_7$ under pressure is proposed. The effects of the Hund's coupling is also discussed.

MODEL AND METHOD

To fully take into account the superexchange couplings, we consider an 11-band Hubbard model [3] that can be written as,

$$H = \sum_{i,j,\alpha,\beta,\sigma} t_{i,j,\alpha,\beta} d_{i\alpha\sigma}^\dagger c_{j\beta\sigma} + \sum_{i,j,\alpha,\beta,\sigma} t_{i,j,\alpha,\beta} c_{i\alpha\sigma}^\dagger c_{j\beta\sigma} + \sum_{i\alpha} (\epsilon_\alpha - \mu) n_{i\alpha}^d + \sum_{i\alpha\sigma} (\epsilon_\alpha - \mu) n_{i\alpha\sigma}^c - \sum_{i\alpha\sigma} E_{dc} n_{i\alpha\sigma}^d + \sum_{i\alpha} U n_{i\alpha\uparrow}^d n_{i\alpha\downarrow}^d + \sum_{i,\alpha<\beta,\sigma} U' n_{i\alpha\sigma}^d n_{i\beta\sigma}^d + (U' - J_H) n_{i\alpha\sigma}^d n_{i\beta\sigma}^d$$

where $t_{i,j,\alpha,\beta}$ denote hoppings between electrons on sites (i, j) and orbital (α, β) (can be either Ni- d or O- p orbitals). $d_{\alpha,i,\sigma}^\dagger$ ($c_{\alpha,i,\sigma}^\dagger$) is the creation operator for electrons on $\alpha \in 3d$ ($\in 2p$) orbital. ϵ_α is the site-energy of α -orbital. U is the Hubbard interaction between two electrons on the same d -orbital ($d_{x^2-y^2}$ or $d_{3z^2-r^2}$) and U' is for that on two different d -orbitals. $U' = U - 2J_H$ is adopted where J_H is the Hund's coupling as following Ref. [48]. E_{dc} is the double counting (DC) term [49–51] to be subtracted in the DQMC or CDMFT. Here we use the Held's formula [52]: $E_{dc} = \frac{1}{3}(U + 2U' - J_H)(n_d^0 - 0.5)$, with n_d^0 being the occupation number of d -orbitals in the non-interacting limit, $n_d^0 \approx 2.16$ in our case (see also the *Appendix*). We adopt the hopping parameters and site-energies proposed in Ref. [3], which is obtained by downfolding the DFT result in the maximally localized Wannier orbitals. See Fig. 1 and Fig. S1 in SI Appendix for all the hopping parameters and site-energy values. In line with DFT result [3], we assume that the chemical potential $\mu = 0$ in above Hamiltonian corresponds to the pristine single crystal $\text{La}_3\text{Ni}_2\text{O}_7$ material at pressures $> 14\text{GPa}$, without considering other potential dop-

ing effects (oxygen deficiency for example). We will also vary μ to explore regimes with different hole concentrations that defined as $n_h = (22 - \sum_{\alpha,\sigma} n_{\alpha,\sigma})/4$, namely, the average number of holes per d -orbitals per site. $n_h = 1$ corresponds to half-filling in our study. In this work, we use $U = 7\text{ eV}$ and $J_H = 0.1U = 0.7\text{ eV}$ unless otherwise stated. Below we use electron volt (eV) as the energy unit throughout the paper. For the calculations on cuprate, we employ a canonical set of parameters for the three-band Hubbard model [42] (one $d_{x^2-y^2}$ orbital and two p_x / p_y orbitals in the CuO_2 plane): $t_{pd} = 1.39, t_{pp} = 0.64, t'_{pp} = 0.103, \Delta_{dp} \equiv \epsilon_d - \epsilon_p = 2.6, U = 8.5, E_{DC} = 3.12$. This set of parameters is assumed to be most relevant for the $\text{La}_{2-x}\text{Sr}_x\text{CuO}_4$ (LSCO) compound, which has been used in studies on different aspects of cuprates [42, 46, 53, 54].

For DQMC simulation, we employ two dimensional square lattices with $6 \times 6 \times 11 = 396$ orbitals at most. For CDMFT study, we carry out computations in the normal state, where an effective impurity model with the $2 \times 2 \times 11 = 44$ orbitals is used. For more details on the methods see the *Appendix*.

RESULTS

Superexchanges

We first discuss the magnetic exchange couplings in the system. As shown in Fig. 1, there are a few hopping processes can give rise to significant superexchanges. In the atomic limit of the charge-transfer picture, the spin singlet state of two Ni- d electrons acquires an energy gain of $J = \frac{-4t_{pd}^4}{(U + \Delta_{pd})^2} \times (\frac{1}{U} + \frac{1}{U + \Delta_{pd}})$ over the spin triplet states, where $\Delta_{pd} = \epsilon_d - \epsilon_p$, and t_{pd} is the hopping between Ni- d and O- p orbitals. The numbers shown in Fig. 2A are the magnitudes of spin correlation function $\langle S_{i,\alpha} \cdot S_{j,\beta} \rangle$ for a few pairs of neighbouring d -orbitals at $T = 0.25$ from DQMC. Here $S_{i,\alpha}$ is the spin operator at site i and orbital α . This result profiles the relative strengths of the main exchange couplings in the system: at $T = 0.25$ and half-filling, the inter-layer (IT) on-site $d_{3z^2-r^2}$ - $d_{3z^2-r^2}$ antiferromagnetic (AFM) exchange dominates the exchange couplings in the system [$\langle S \cdot S \rangle = -0.082(2)$]. Then it comes the intra-layer (IR) nearest-neighboring $d_{x^2-y^2}$ - $d_{x^2-y^2}$ exchange [$\langle S \cdot S \rangle = -0.050(1)$]. The intra-layer $d_{3z^2-r^2}$ - $d_{x^2-y^2}$ superexchange is weaker than the aforementioned two [$\langle S \cdot S \rangle = -0.029(1)$]. Finally, the intra-layer $d_{3z^2-r^2}$ - $d_{3z^2-r^2}$ exchange is found the weakest among those couplings. In particular, in CDMFT at $T = 0.08$ and $\mu = 0$ (Fig. 2C), the intra-layer $d_{3z^2-r^2}$ - $d_{3z^2-r^2}$ correlation is less than 1/20 of the inter-layer $d_{3z^2-r^2}$ - $d_{3z^2-r^2}$ correlation, hence it can be neglected in future studies on $\text{La}_3\text{Ni}_2\text{O}_7$ (which corresponds to $\mu = 0$ in our study). Fig. 2B and 2D show $\langle S_{i,\alpha} \cdot S_{j,\beta} \rangle$ as a

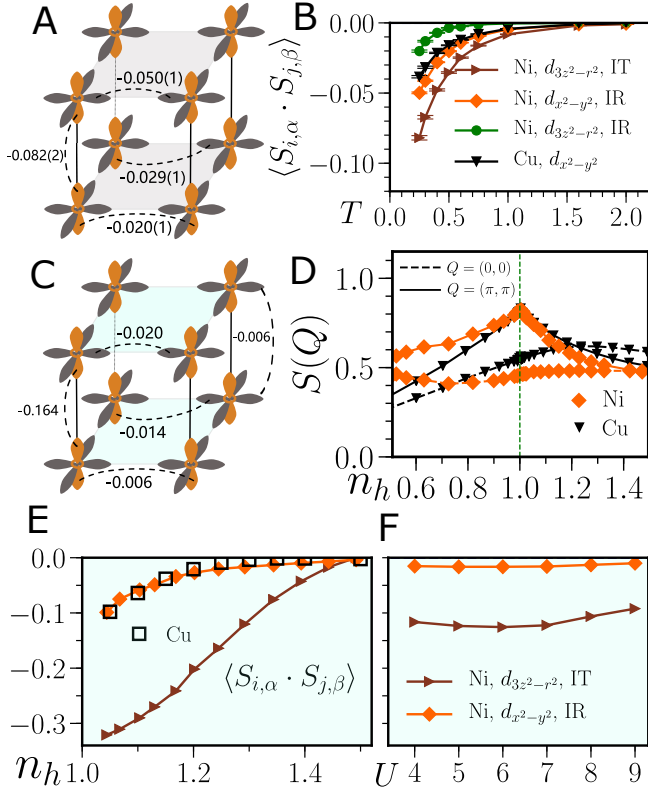


FIG. 2. Magnetic correlations between d -orbitals due to the superexchanges in the 11-band Hubbard model. **A,C**: The spin-spin correlation function $\langle S_{i,\alpha} \cdot S_{j,\beta} \rangle$ for four neighboring d -orbitals are shown in numbers to profile the relative strength of the antiferromagnetic superexchange couplings in the system. Brown (Gray) symbols denote $d_{3z^2-r^2}$ ($d_{x^2-y^2}$) orbitals. **A** and **C** are respectively from DQMC at half-filling ($n_h = 1$), $T = 0.25$, and from CDMFT at $\mu = 0$ ($n_h \approx 1.244$), $T = 0.08$. Note that here the magnetic correlations between the onsite $d_{x^2-y^2}$ - $d_{3z^2-r^2}$ orbitals due to Hund's coupling are not shown. **B**: $\langle S_{i,\alpha} \cdot S_{j,\beta} \rangle$ between pairs of nearest neighbouring (NN) d orbitals in Ni-11-band and Cu-3-band model as a function of temperature T at half-filling from DQMC. Diamonds show result for intra-layer (IR) $d_{x^2-y^2}$ - $d_{x^2-y^2}$ correlations, while triangles denote that between the inter-layer (IT) $d_{3z^2-r^2}$ - $d_{3z^2-r^2}$ orbitals. **D**: The spin structure factor $S(Q) = \frac{1}{N} \sum_{i,j} \langle S_{i,\alpha} \cdot S_{j,\beta} \rangle e^{-iQ \cdot (R_i - R_j)}$ for Ni (intra-layer, *i.e.*, $\alpha = \beta = d_{x^2-y^2}$ component) as a function of hole concentration n_h compared with that of cuprate. **E**: $\langle S_{i,\alpha} \cdot S_{j,\beta} \rangle$ as a function of n_h from CDMFT at $T = 0.08$. **F**: Same as E but result is shown as a function of Hubbard U ($J_H = 0.1U$) at $n_h = 1.25$ ($\mu \sim 0$). Here $U = 7$, $J_H = 1.05$ for nickelate and $U = 8.5$ for cuprate unless otherwise stated. In DQMC, we use $6 \times 6 \times 11$ orbitals for Ni and $6 \times 6 \times 3$ orbitals for Cu.

function of temperature at half-filling, and spin structure factor $S_{\alpha,\beta}(Q)$ as a function of n_h at $T = 0.3$ respectively, comparing with the result of the 3-band Hubbard model of cuprates. As one can see that the intra-layer $d_{x^2-y^2}$ - $d_{x^2-y^2}$ correlation in the 11-band Hubbard model is in general comparable to its cuprate counterpart. The inter-layer $d_{3z^2-r^2}$ - $d_{3z^2-r^2}$ correlation, on the

other hand, seems to be essentially stronger the $d_{x^2-y^2}$ - $d_{x^2-y^2}$ correlations. This result implies that the AFM correlations between inter-layer $d_{3z^2-r^2}$ orbitals could be at the origin of the observed superconductivity in $\text{La}_3\text{Ni}_2\text{O}_7$ under pressure. Fig. 2E and 2F show respectively $\langle S_{i,\alpha} \cdot S_{j,\beta} \rangle$ as a function of n_h at $U = 7$, and as a function of U at $n_h = 1.25$ (where $\mu \sim 0$) in CDMFT. Here one sees that varying the value of U in the range of (4 ~ 9) eV does not change substantially the interlayer $d_{3z^2-r^2}$ - $d_{3z^2-r^2}$ magnetic correlation at $\mu \sim 0$ (Fig. 2F). More importantly, as shown in Fig. 2E, the interlayer $d_{3z^2-r^2}$ - $d_{3z^2-r^2}$ AFM correlation does not vanish unless a huge hole doping $p = n_h - 1 \gtrsim 0.45$ is approached. We find that despite the fact that Hund's coupling J_H in principle can transfer the magnetic correlations between the vertical $d_{3z^2-r^2} - d_{3z^2-r^2}$ bonds to other orbitals, the overall effects seem to be negligible in our study. For example, as shown in Fig. 2C, $\langle S \cdot S \rangle$ between interlayer $d_{x^2-y^2} - d_{x^2-y^2}$ orbitals are tiny (~ -0.006) as compared to that of the $d_{3z^2-r^2} - d_{3z^2-r^2}$ orbitals. This may be attributed to the small effective filling factors of the in-plane orbitals, namely, the in-plane $d_{x^2-y^2}$ and p_x/p_y orbitals are less affected by the Hund's coupling due to their large itinerancy, as to be shown below.

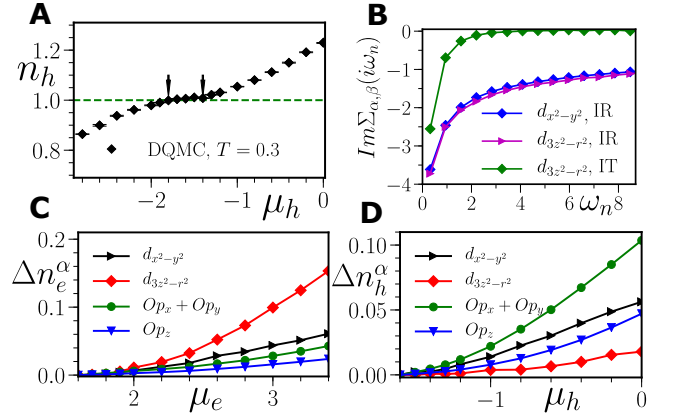


FIG. 3. Charge transfer insulating behaviour of the 11-band Hubbard at half-filling. **A**: The hole concentration n_h as a function of hole chemical potential μ_h . DQMC result of n_h at $T = 0.3$ suggests that a charge gap opens as hole chemical potential approaches $\mu_h \sim -1.6$. Black arrows indicate the μ_h range where $n_h \approx 1$. **B**: Imaginary part of the self-energies from DMFT at half-filling $n_h \approx 1$ and $T = 0.1$. **C**: The change of electron concentration Δn_e^α for different orbital- α as a function of electron chemical potential μ_e for $\mu_e > 1.6$ (where $n_e > 1$, electron-doped). Δn_e^α is defined as $\Delta n_e^\alpha \equiv n_e^\alpha(\mu_e) - n_e^\alpha(\mu_e = 1.6)$, where $n_e^\alpha(\mu_e = 1.6) \approx 1$ is the electron filling of orbital- α at $\mu_e = -\mu_h = 1.6$ ($n_e = \sum_\alpha n_e^\alpha$). **D**: Result similar to C but for Δn_h^α in hole doping regime ($\mu_h > -1.6$, $n_h = 2 - n_e > 1$). C and D use same method and same parameters as A. See also main text.

Charge transfer insulator

We now focus on the metal- insulator transition in the 11-band Hubbard model. Fig. 3A displays the hole concentration per d orbital n_h as a function of hole chemical potential $\mu_h \equiv -\mu$. As one can see that the DQMC result (dots) of n_h at $T = 0.3$ exhibits almost a plateau at $n_h = 1$ ($\mu_h \sim -1.6$) with a vanishing compressibility $\partial n_h / \partial \mu_h$, suggesting the opening of a charge gap at half-filling. CDMFT result on the imaginary part of the self-energies obtained at lower temperature shown in Fig. 3B also points to the insulating nature of the 11-band Hubbard model at half-filling. To understand the nature of this insulating state, we further study how the hole/electron concentration changes in different orbitals as a function of chemical potentials in Fig. 3C and Fig. 3D respectively. In other words, as hole chemical potential $\mu_h \equiv -\mu$ and electron chemical potential $\mu_e \equiv \mu$ are increased from their half-filled values $\mu_h = -\mu_e \sim -1.6$, holes/electrons can be added into different Ni- d and O- p orbitals of the system, which is denoted by $\Delta n_{e/h}^\alpha$ in Fig. 3C and Fig. 3D. As one can see that the doped holes go primarily to the oxygen p - orbitals (Fig. 3D), while the doped electrons reside mainly on the nickel d - orbitals (Fig. 3C), which unambiguously indicates the charge-transfer nature [44] of the insulating state of this system at half-filling. Similar to cuprates [46], here $d_{x^2-y^2}$ orbital has a sizable portion of doped holes in the case of hole doping ($\mu_h > -1.6$). It is remarkable that, as shown in Fig. 3D, Δn_h^α of $d_{3z^2-r^2}$ orbital are much smaller than that of $d_{x^2-y^2}$ orbital in the hole doped regime at given μ_h , reflecting the fact the $d_{3z^2-r^2}$ orbital is more strongly correlated than the $d_{x^2-y^2}$ orbital at hole doping. See more discussions below. We note that in cuprates, a smaller portion of holes residing on cations in general indicates a larger superexchange coupling [46, 55].

Zhang-Rice singlet band

In Fig. S7A, we plot the local density of states (DOS) $\rho(\omega)$ for Ni- $d_{3z^2-r^2}$, and for the out-of-plane O- p_z orbital at $n_h \approx 1.035, T = 0.08$, where we see that the overall structure of $\rho(\omega)$ resembles that of the underdoped cuprate [46]: the well-separated lower and upper Hubbard bands (LHB/UHB) appear in the Ni DOS. There is a central band with mixed weights of Ni- d and O- p orbitals that can be called the charge-transfer band(CTB) [46]. More importantly, the DOS of Ni- $d_{3z^2-r^2}$ and O- p_z near Fermi level form a narrow band separated from the upper Hubbard band by a charge-transfer gap (CTG). In the context of cuprate, this low-energy band is usually referred to as the Zhang-Rice singlet band (ZRSB) [45]. Similar result of the in-plane Ni- $d_{x^2-y^2}$ and O- p_x/p_y orbitals is shown in Fig. S7B, where

the low-energy singlet band has a wider bandwidth compared to its out-of-plane counterpart shown in Fig. S7A, suggesting a less localized nature of the in-plane orbitals.

There are a few points we would like to emphasize. First, the vertical $d_{3z^2-r^2}$ - p_z singlet band can be quite different from a conventional ZRSB. In cuprates, a doped hole at oxygen sites hybridize with a Cu^{2+} hole in terms of the superposition of four O_p hole states adjacent to the Cu^{2+} iron, forming a spin singlet. The spin singlet moves effectively in the antiferromagnetic background of Cu^{2+} lattice with an effective bandwidth being ($2 \sim 3$)eV [46]. Here the vertical singlet states of Ni- $d_{3z^2-r^2}$ -O- p_z have a narrow bandwidth, and they barely interact with each other directly. Instead, the in-plane holes hybridize with the vertical singlets via $d_{3z^2-r^2}$ - p_x/p_y hopping ($t_2 = 0.75$), or via the p_x - p_z hopping ($t_5 = 0.49, t_7 = 0.43$, see Fig. 1). As a result, the vertical $d_{3z^2-r^2}$ singlet band may behave more like scattering centers with antiferromagnetic characteristics in the system. On the other hand, one can expect that the in-plane ZRSB associated with the $d_{x^2-y^2}$ and p_x/p_y orbitals could draw a close analogue to the ZRSB in cuprate. However, as exemplified in Fig. S7D for $n_h \approx 1.244$ ($\mu = 0$), the in-plane orbitals become itinerant and the charge-transfer gap is essentially absent at this large hole concentration. Hence, whether the concept of ZRSB still applies in capturing the in-plane single particle excitations in $\text{La}_3\text{Ni}_2\text{O}_7$ is in question. It is remarkable that, nevertheless, the vertical singlet band as shown in Fig. S7C, remains intact at this large $n_h \approx 1.244$.

	n_h	n_h^{IP}	n_h^{OP}
DQMC ($U = 7, T = 0.25$)	1.233	1.400	1.065
CDMFT ($U = 7, T = 0.08$)	1.244	1.434	1.054
CDMFT ($U = 7^*, T = 0.1$)	1.256	1.443	1.069
CDMFT ($U = 9^*, T = 0.1$)	1.216	1.385	1.048

TABLE I. Hole concentrations at $\mu_h = -\mu = 0$. The last two results starred out are obtained with $U' = 0.7U, J_H = 0$, *i.e.*, there is no Hund's coupling.

Now we focus on the distribution of holes in different orbitals. As discussed above, considering the formation out-of-plane (in-plane) spin singlet states, it is judicious to consider the carriers in the $d_{3z^2-r^2}$ and p_z ($d_{x^2-y^2}$ and p_x/p_y) orbitals as a whole, which are represented by the out-of-plane hole concentration n_h^{OP} (in-plane hole concentration n_h^{IP}) in Fig. 5. In Fig. 5, we see that the out-of-plane hole doping level $p = n_h^{OP} - 1$ (dots) is always small while μ_h is varied in the range of $(0, -2)$. In other words, the out-of-plane orbitals as a whole is always underdoped ($|n_h^{OP} - 1| < 7\%$) in this chemical potential range. The in-plane orbitals, in contrast, can be heavily overdoped, as denoted by a large value of $(n_h^{IP} - 1)$ (diamonds) when $\mu_h \sim 0$. In Table-I we inspect specifically the hole concentration levels at $\mu = 0$, which is

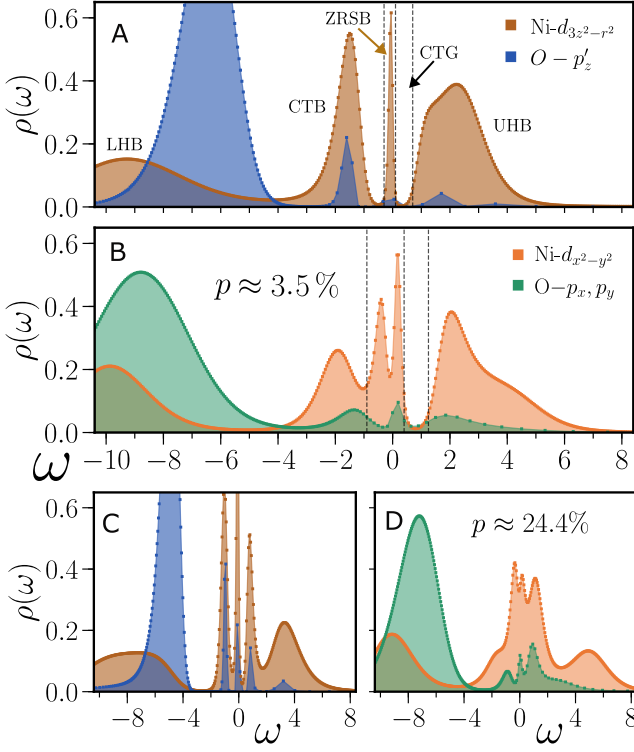


FIG. 4. Local density of states (DOS). **A:** DOS of the out-of-plane $d_{3z^2-r^2}$ and p'_z orbitals. Here $n_h \approx 1.045$ hence $p = n_h - 1 \approx 3.5\%$. **B:** DOS of the in-plane $d_{x^2-y^2}$ and p_x (p_y) orbitals. Dashed vertical lines indicate the Zhang-Rice singlet band (ZRSB) and the charge-transfer gap (CTG). UHB stands for upper Hubbard band, and LHB stands for lower Hubbard band. **C:** The same as A but $p \approx 24.4\%$ ($\mu = 0$). **D:** The same as B but $p \approx 24.4\%$. DOS are obtained by maximum entropy (MEM) analytic continuation [56] of the Matsubara Green's functions that obtained by CDMFT at $T = 0.08, U = 7, U' = 0.8U, J_H = 0.1U$. Similar results can be seen in Fig. S2 in Appendix at different Hubbard U and temperature T .

assumed to correspond to that of the real material of $\text{La}_3\text{Ni}_2\text{O}_7$ under pressure. As one sees that, in our study the 11-band Hubbard model is about $p = 22 \sim 26\%$ hole doped at $\mu = 0$. Changing methods or varying the values of Hubbard U , Hund's coupling J_H or temperatures T do not significantly change the value of p . This result roughly coincides with the nominal doping level of the e_g orbitals in $\text{La}_3\text{Ni}_2\text{O}_7$ ($p = 25\%$). Table-I also shows that at $\mu = 0$, the hole doping in the out-of-plane orbitals is around $p = (n_h^{OP} - 1) \approx (5\% \sim 7\%)$, while for that of the in-plane orbitals, $p = (n_h^{IP} - 1)$ is about $\approx 40\%$ at different Hubbard U and temperature T . The stark inhomogeneous distribution of the holes in the two different e_g orbitals (and their correlated O- p orbitals) explains the finding in Fig. S7 that the vertical low-energy singlet band remains strongly correlated at large p while the in-plane low-energy DOS displays great itinerancy. A natural question is that whether the in-plane $d_{x^2-y^2}$

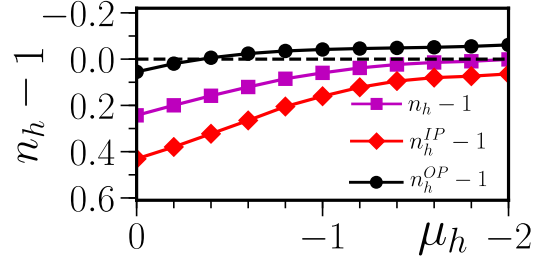


FIG. 5. Hole concentrations as functions of chemical potential μ_h . Here $n_h^{IP} = n_{d_{x^2-y^2}}^h + n_{p_x}^h + n_{p_y}^h$ counts the number of holes in the in-plane $d_{x^2-y^2}$ orbital and p_x / p_y orbitals combined, while $n_h^{OP} = n_{d_{3z^2-r^2}}^h + 0.5(n_{p_z}^h + n_{p_z'}^h)$ counting the number of holes in the out-of-plane orbitals. $n_h = (n_h^{IP} + n_h^{OP})/2$. Thus $n_h - 1$ is the hole doping from half-filling of the system. Note that as μ_h approaches $\mu_h = -2$, $n_h - 1$ curve becomes flat, indicating the opening of a charge gap at half-filling.

and p_x/p_y orbitals can be seen as pure itinerant orbitals without interaction terms in $\text{La}_3\text{Ni}_2\text{O}_7$? We find that in CDMFT at $n_h \sim 1.25$, the magnetic correlation between intra-layer $d_{x^2-y^2} - d_{x^2-y^2}$ orbitals is weak but not vanishing (see Fig. 2E). It is notable that the strange metal (SM) phase can be very sensitive to weak magnetic correlations [57]. Hence, if the observed strange metal state in $\text{La}_3\text{Ni}_2\text{O}_7$ at $P > 18\text{GPa}$ is also related to the magnetic correlations in $d_{x^2-y^2}$ orbitals, then the latter may not be simplified as pure itinerant.

Effective t-J model

Based on our study above, we propose a four-band $t - J$ model to describe the low-energy physics of the $\text{La}_3\text{Ni}_2\text{O}_7$ under pressure. The proposed Hamiltonian can be written as $\mathcal{H} = \mathcal{H}_0 + \mathcal{H}_J$, with the non-interacting $\mathcal{H}_0 = \sum_{k\sigma} \Psi_{k\sigma}^\dagger H(k) \Psi_{k\sigma}$ written as,

$$\begin{aligned}
 H(k)_{1,1} &= H(k)_{3,3} = -2t_1^x [\cos(k_x) + \cos(k_y)] \\
 &\quad -4t_2^x \cos(k_x) \cos(k_y) + \epsilon_x \\
 H(k)_{2,2} &= H(k)_{4,4} = -2t_1^z [\cos(k_x) + \cos(k_y)] \\
 &\quad -4t_2^z \cos(k_x) \cos(k_y) + \epsilon_z \\
 H(k)_{1,2} &= H(k)_{3,4} = -2t^{xz} [\cos(k_x) - \cos(k_y)] \\
 H(k)_{2,4} &= -2V_\perp [\cos(k_x) - \cos(k_y)] \quad (2)
 \end{aligned}$$

where $\Psi_\sigma = (d_{x_1\sigma}, d_{z_1\sigma}, d_{x_1\sigma}, d_{z_2\sigma})^T$, denoting the annihilation operators of $d_{x^2-y^2}$ and $d_{3z^2-r^2}$ orbitals in the two NiO_2 layer, while the oxygen degrees of freedom have been integrated out. The \mathcal{H}_0 part is taken from the down-folded tight-binding model from Luo *et al's* work in Ref. [3], namely, $t_1^x \approx 0.5, t_2^x \approx 0.07, t_1^z \approx 0.11, t_2^z \approx 0.02, t^{xz} = -0.24, V_\perp = 0.64$.

For the interacting part \mathcal{H}_J , we consider three main magnetic exchanges terms,

$$\begin{aligned} \mathcal{H}_J = & J_1 \sum_i (S_{i,z_1} S_{i,z_2} - \frac{1}{4} n_{i,z_1} n_{i,z_2}) \\ & + J_2 \sum_{\langle i,j \rangle, \alpha=x_1, x_2} (S_{i,\alpha} S_{j,\alpha} - \frac{1}{4} n_{i,\alpha} n_{j,\alpha}) \\ & + J_3 \sum_{\substack{\langle i,j \rangle \\ (\alpha,\beta)=(x_1,z_1)/(x_2,z_2)}} (S_{i,\alpha} S_{j,\beta} - \frac{1}{4} n_{i,\alpha} n_{j,\beta}) \end{aligned} \quad (3)$$

where J_1 captures the exchange couplings between the on-site inter-layer $d_{3z^2-r^2}$ orbitals, J_2 the exchanges between the intra-layer $d_{x^2-y^2}$ orbitals on nearest neighboring (NN) sites, and finally J_3 for the intra-layer $d_{x^2-y^2}$ - $d_{3z^2-r^2}$ exchanges on NN sites. Considering the superexchange coupling calculated in the atomic limit with $U = 7$, and the magnetic correlation results compared with LSCO cuprate [59, 60], typical value of J_1 can be chosen as, for example, $J_1 \sim 0.18\text{eV}$ (see *Appendix*). The values of J_2, J_3 should be in principle smaller than J_1 . The arbitrariness of adopting the values of these J s, however, can not be eliminated without further experimental researches. The magnetic couplings between the on-site interlayer $d_{x^2-y^2} - d_{3z^2-r^2}$ and interlayer $d_{x^2-y^2} - d_{x^2-y^2}$ orbitals may also be further added in Eq. 3 when Hund's coupling J_H [58] is taken into account.

DISCUSSION AND CONCLUSION

After the discovery of high- T_c superconductivity in $\text{La}_3\text{Ni}_2\text{O}_7$ under pressure [2], a number of effective interacting models have been proposed to study the pairing symmetry [61–64], as inspired by the *ab initio* calculations [3, 65–68] or phenomenological insights. These effective models ignore the oxygen degrees of freedom, incorporating the magnetic correlations between Ni orbitals in terms of direct exchanges. Hence, the charge transfer property, which has shown to be one of the key ingredients in determining T_c of cuprate superconductors [42, 46, 55, 69, 70], as well as the superexchange couplings, are beyond the scope of those effective models. In this work, we have studied an 11-band Hubbard model including both Ni- $3d$ orbitals and relevant O- $2p$ orbitals. We reveal the relative strengths of the superexchange couplings between different Ni- $3d$ orbitals. We find two spin-singlet bands in the system possessing strikingly different hole concentrations and correlation strengths. These results suggest that the strong antiferromagnetic correlations within the inter-layer $d_{3z^2-r^2}$ orbitals might be the driving force of the SC in $\text{La}_3\text{Ni}_2\text{O}_7$. The role of the more itinerant $d_{x^2-y^2}$ orbital in SM and SC states, owing to the small but not vanishing remnant magnetic correlations within, and the specific geometry

of the α, β - sheets of the Fermi surface [3], might be complicated and requires further investigations. Finally, we note that an experimental work [37] probing the optical response in $\text{La}_3\text{Ni}_2\text{O}_7$ reveals the proximity to Mottness of the electron correlations. This finding is in accordance with our doped charge-transfer insulator description of the $\text{La}_3\text{Ni}_2\text{O}_7$ under pressure.

ACKNOWLEDGEMENTS

We thank Hualei Sun, Mi Jiang, K. Le Hur, Yi Lu, and Xunwu Hu for useful discussions. W.W is indebted to A. -M. Tremblay for useful discussions and insightful suggestions. W.W. acknowledge help from Dong Meng in preparing the illustrations in Figure 1. Work at Sun Yat-sen University was supported by the National Natural Science Foundation of China (Grants No.12274472, No. 92165204, No.12174454, No.11974432), the National Key Research and Development Program of China (Grants No. 2022YFA1402802, 2018YFA0306001), the Guangdong Basic and Applied Basic Research Foundation (Grants No. 2022A1515011618, No. 2021B1515120015), Guangdong Provincial Key Laboratory of Magnetoelectric Physics and Devices (Grant No. 2022B1212010008), Shenzhen International Quantum Academy (Grant No. SIQA202102), and Leading Talent Program of Guangdong Special Projects (201626003). We acknowledge the support from Guangzhou National Supercomputing Center (Tianhe-II).

* wuwei69@mail.sysu.edu.cn

- [1] Bednorz JG, Müller KA (1986) Possible high t_c superconductivity in the ba- la- cu- o system. *Zeitschrift für Physik B Condensed Matter* 64(2):189–193.
- [2] Sun H, et al. (2023) Superconductivity near 80 kelvin in single crystals of $\text{La}_3\text{Ni}_2\text{O}_7$ under pressure. *Nature* 621:493–498.
- [3] Luo Z, Hu X, Wang M, Wu W, Yao DX (2023) Bilayer two-orbital model of $\text{la}_3\text{ni}_2\text{o}_7$ under pressure. *Phys. Rev. Lett.* 131 126001
- [4] Zhang FC, Rice TM (1988) Effective hamiltonian for the superconducting cu oxides. *Phys. Rev. B* 37(7):3759–3761.
- [5] Kotliar G (1988) Resonating valence bonds and d-wave superconductivity. *Phys Rev B Condens Matter* 37(7):3664–3666.
- [6] Emery V, Kivelson S (1995) Importance of phase fluctuations in superconductors with small superfluid density. *Nature* 374(6521):434–437.
- [7] Scalapino DJ (2007) Numerical studies of the 2D Hubbard model in *Handbook of High-Temperature Superconductivity: Theory and Experiment*, eds. Schrieffer JR, Brooks JS. (Springer New York), pp. 495–526.
- [8] Keimer B, Kivelson SA, Norman MR, Uchida S, Zaanen J (2015) From quantum matter to high-temperature su-

- perconductivity in copper oxides. *Nature* 518(7538):179–186.
- [9] Maeno Y, et al. (1994) Superconductivity in a layered perovskite without copper. *nature* 372(6506):532–534.
- [10] Kamihara Y, et al. (2006) Iron-based layered superconductor: LaOFeP. *Journal of the American Chemical Society* 128(31):10012–10013.
- [11] Maeno Y, Rice TM, Sigrist M (2001) The intriguing superconductivity of strontium ruthenate. *Physics Today* 54(1):42–47.
- [12] Chen X, et al. (2008) Superconductivity at 43 k in $\text{SmFeAsO}_{1-x}\text{F}_x$. *nature* 453(7196):761–762.
- [13] Chubukov AV, Efremov DV, Eremin I (2008) Magnetism, superconductivity, and pairing symmetry in iron-based superconductors. *Phys. Rev. B* 78(13):134512.
- [14] Hu J, Le C, Wu X (2015) Predicting unconventional high-temperature superconductors in trigonal bipyramidal coordinations. *Physical Review X* 5(4):041012.
- [15] Kitatani M, et al. (2023) Optimizing superconductivity: From cuprates via nickelates to palladates. *Phys. Rev. Lett.* 130(16):166002.
- [16] Jiang S, Scalapino DJ, White SR (2021) Ground-state phase diagram of the t-t'-j model. *Proceedings of the National Academy of Sciences* 118(44):e2109978118.
- [17] Christos M, et al. (2023) A model of d-wave superconductivity, antiferromagnetism, and charge order on the square lattice. *Proceedings of the National Academy of Sciences* 120(21):e2302701120.
- [18] Li D, et al. (2019) Superconductivity in an infinite-layer nickelate. *Nature* 572(7771):624–627.
- [19] Lee KW, Pickett WE (2004) Infinite-layer LaNiO_2 : Ni^{1+} is not Cu^{2+} . *Phys. Rev. B* 70(16):165109.
- [20] Middey S, et al. (2016) Physics of ultrathin films and heterostructures of rare-earth nickelates. *Annual Review of Materials Research* 46:305–334.
- [21] Haule K, Pascut GL (2017) Mott transition and magnetism in rare earth nickelates and its fingerprint on the x-ray scattering. *Scientific reports* 7(1):1–7.
- [22] Peil OE, Hampel A, Ederer C, Georges A (2019) Mechanism and control parameters of the coupled structural and metal-insulator transition in nickelates. *Phys. Rev. B* 99(24):245127.
- [23] Jiang M, Berciu M, Sawatzky GA (2020) Critical nature of the Ni spin state in doped NdNiO_2 . *Physical Review Letters* 124(20):207004.
- [24] Botana AS, Norman MR (2020) Similarities and differences between LaNiO_2 and CaCuO_2 and implications for superconductivity. *Phys. Rev. X* 10(1):011024.
- [25] Zhang GM, Yang Yf, Zhang FC (2020) Self-doped mott insulator for parent compounds of nickelate superconductors. *Phys. Rev. B* 101(2):020501.
- [26] Werner P, Hoshino S (2020) Nickelate superconductors: Multiorbital nature and spin freezing. *Phys. Rev. B* 101(4):041104.
- [27] Wang Y, Kang CJ, Miao H, Kotliar G (2020) Hund's metal physics: From SrNiO_2 to LaNiO_2 . *Phys. Rev. B* 102(16):161118.
- [28] Lechermann F (2020) Multiorbital processes rule the $\text{Nb}_{1-x}\text{Sr}_x\text{NiO}_2$ normal state. *Phys. Rev. X* 10(4):041002.
- [29] Worm P, et al. (2022) Correlations tune the electronic structure of pentalayer nickelates into the superconducting regime. *Phys. Rev. Mater.* 6(9):L091801.
- [30] Gu Q, et al. (2020) Single particle tunneling spectrum of superconducting $\text{Nd}_{1-x}\text{Sr}_x\text{NiO}_2$ thin films. *Nature communications* 11(1):6027.
- [31] Chen H, Hampel A, Karp J, Lechermann F, Millis AJ (2022) Dynamical mean field studies of infinite layer nickelates: Physics results and methodological implications. *Frontiers in Physics* 10:16.
- [32] Ding X, et al. (2023) Critical role of hydrogen for superconductivity in nickelates. *Nature* 615(7950):50–55.
- [33] Pardo V, Pickett WE (2011) Metal-insulator transition in layered nickelates $\text{La}_3\text{Ni}_2\text{O}_{7-\delta}$ ($\delta = 0.0, 0.5, 1$). *Phys. Rev. B* 83(24):245128.
- [34] Liu Z, et al. (2023) Evidence for charge and spin density waves in single crystals of $\text{La}_3\text{Ni}_2\text{O}_7$ and $\text{La}_3\text{Ni}_2\text{O}_6$. *Science China Physics, Mechanics & Astronomy* 66(1):217411.
- [35] Gao M, Lu Z, Xiang T (2015) Finding high-temperature superconductors by metallizing the σ -bonding electrons. *PHYSICS* 44(7):421–426.
- [36] Lu H, et al. (2021) Magnetic excitations in infinite-layer nickelates. *Science* 373(6551):213–216.
- [37] Liu Z, et al. (2023) Electronic correlations and energy gap in the bilayer nickelate $\text{La}_3\text{Ni}_2\text{O}_7$. *arXiv:2307.02950*.
- [38] Blankenbecler R, Scalapino D, Sugar R (1981) Monte carlo calculations of coupled boson-fermion systems. i. *Physical Review D* 24(8):2278.
- [39] Assaad F, Evertz H (2008) World-line and determinantal quantum monte carlo methods for spins, phonons and electrons. *Computational Many-Particle Physics* pp. 277–356.
- [40] Georges A (1996) Dynamical mean-field theory of strongly correlated fermion systems and the limit of infinite dimensions. *Reviews of Modern Physics* 68.
- [41] Maier T, Jarrell M, Pruschke T, Hettler MH (2005) Quantum cluster theories. *Rev. Mod. Phys.* 77(3):1027–1080.
- [42] Weber C, Yee C, Haule K, Kotliar G (2012) Scaling of the transition temperature of hole-doped cuprate superconductors with the charge-transfer energy. *Europhysics Letters* 100(3):37001.
- [43] Karp J, et al. (2020) Many-body electronic structure of NdNiO_2 and CaCuO_2 . *Phys. Rev. X* 10(2):021061.
- [44] Zaanen J, Sawatzky GA, Allen JW (1985) Band gaps and electronic structure of transition-metal compounds. *Phys. Rev. Lett.* 55(4):418–421.
- [45] Zhang F, Rice T (1988) Effective hamiltonian for the superconducting Cu oxides. *Physical Review B* 37(7):3759.
- [46] Kowalski N, Dash SS, Sémon P, Sénéchal D, Tremblay AM (2021) Oxygen hole content, charge-transfer gap, covalency, and cuprate superconductivity. *Proceedings of the National Academy of Sciences* 118(40):e2106476118.
- [47] O'Mahony SM, et al. (2022) On the electron pairing mechanism of copper-oxide high temperature superconductivity. *Proceedings of the National Academy of Sciences* 119(37):e2207449119.
- [48] Held K, Keller G, Eyert V, Vollhardt D, Anisimov VI (2001) Mott-hubbard metal-insulator transition in paramagnetic v_2o_3 : An l d a+ d m f t (qmc) study. *Physical review letters* 86(23):5345.
- [49] Anisimov VI, Zaanen J, Andersen OK (1991) Band theory and mott insulators: Hubbard u instead of stoner i. *Phys. Rev. B* 44(3):943–954.
- [50] Karolak M, et al. (2010) Double counting in l d a+ d m f t—the example of NiO . *Journal of Electron Spectroscopy and Related Phenomena* 181(1):11–15.
- [51] Wang X, et al. (2012) Covalency, double-counting, and the metal-insulator phase diagram in transition metal ox-

- ides. Phys. Rev. B 86(19):195136.
- [52] Held K (2007) Electronic structure calculations using dynamical mean field theory. Advances in physics 56(6):829–926.
- [53] Kung Y, et al. (2016) Characterizing the three-orbital hubbard model with determinant quantum monte carlo. Physical Review B 93(15):155166.
- [54] Mai P, Balduzzi G, Johnston S, Maier TA (2021) Pairing correlations in the cuprates: A numerical study of the three-band hubbard model. Physical Review B 103(14):144514.
- [55] Ruan W, et al. (2016) Relationship between the parent charge transfer gap and maximum transition temperature in cuprates. Science bulletin 61:1826–1832.
- [56] Bergeron D, Tremblay AMS (2016) Algorithms for optimized maximum entropy and diagnostic tools for analytic continuation. Phys. Rev. E 94(2):023303.
- [57] Wú W, Wang X, Tremblay AM (2022) Non-fermi liquid phase and linear-in-temperature scattering rate in overdoped two-dimensional hubbard model. Proceedings of the National Academy of Sciences 119(13):e2115819119.
- [58] De’Medici L, Mravlje J, Georges A (2011) Janus-faced influence of hund’s rule coupling in strongly correlated materials. Physical review letters 107(25):256401.
- [59] Wakimoto S, et al. (2007) Disappearance of antiferromagnetic spin excitations in overdoped $La_{2-x}Sr_xCuO_4$. Physical review letters 98(24):247003.
- [60] Wang L, et al. (2022) Paramagnons and high-temperature superconductivity in a model family of cuprates. Nature Communications 13(1):3163.
- [61] Yang QG, Liu HY, Wang D, Wang QH (2023) Possible s_{\pm} -wave superconductivity in $La_{0.3}Ni_{0.2}O_{0.7}$. arXiv preprint arXiv:2306.03706.
- [62] Shen Y, Qin M, Zhang GM (2023) Effective bi-layer model hamiltonian and density-matrix renormalization group study for the high- T_c superconductivity in $La_{1-3x}Ni_{2x}O_{7-7x}$ under high pressure. arXiv preprint arXiv:2306.07837.
- [63] Gu Y, Le C, Yang Z, Wu X, Hu J (2023) Effective model and pairing tendency in bilayer ni-based superconductor $La_{0.3}Ni_{0.2}O_{0.7}$. arXiv preprint arXiv:2306.07275.
- [64] Sakakibara H, Kitamine N, Ochi M, Kuroki K (2023) Possible high T_c superconductivity in $La_{0.3}Ni_{0.2}O_{0.7}$ under high pressure through manifestation of a nearly-half-filled bilayer hubbard model. arXiv preprint arXiv:2306.06039.
- [65] Zhang Y, Lin LF, Moreo A, Dagotto E (2023) Electronic structure, orbital-selective behavior, and magnetic tendencies in the bilayer nickelate superconductor $La_{0.3}Ni_{0.2}O_{0.7}$ under pressure. arXiv preprint arXiv:2306.03231.
- [66] Lechermann F, Gondolf J, Bötzel S, Eremin IM (2023) Electronic correlations and superconducting instability in $La_{0.3}Ni_{0.2}O_{0.7}$ under high pressure. arXiv preprint arXiv:2306.05121.
- [67] Christiansson V, Petocchi F, Werner P (2023) Correlated electronic structure of $La_{0.3}Ni_{0.2}O_{0.7}$ under pressure. arXiv preprint arXiv:2306.07931.
- [68] Shilenko D, Leonov I (2023) Correlated electronic structure, orbital-selective behavior, and magnetic correlations in double-layer $La_{0.3}Ni_{0.2}O_{0.7}$ under pressure. arXiv preprint arXiv:2306.14841.
- [69] Rybicki D, Jurkutat M, Reichardt S, Kapusta C, Haase J (2016) Perspective on the phase diagram of cuprate high-temperature superconductors. Nature communications 7(1):11413.
- [70] O’Mahony SM, et al. (2022) On the electron pairing mechanism of copper-oxide high temperature superconductivity. Proceedings of the National Academy of Sciences 119(37):e2207449119.

APPENDIX

METHODS

For DQMC simulation, we use a two dimensional $6 \times 6 \times 11 = 396$ orbitals square lattice with periodic conditions for the 11-band Hubbard model, on which we have verified that the finite size effects are negligible in the parameter regime we study (See SI Appendix, Fig. S3). In DQMC we use $\Delta\tau = 0.0625$. For CDMFT study, we carry out computations in the normal state, where the $2 \times 2 \times 11 = 44$ orbitals cluster effective impurity model is used. At high temperatures, we find excellent agreement between the DQMC and CDMFT result (see Fig. S9). The Hirsch-Fye quantum Monte Carlo (HFQMC) is used as impurity solver in CDMFT, where $\Delta\tau = 0.078$ is adopted.

We note that in our study, due to the fact that n_d^0 is

$$\begin{aligned}
 H_0(1, 5) = H_0(3, 7) &= -2i * t_1 \sin(0.5k_x) & H_0(1, 6) = H_0(3, 8) &= 2i * t_1 \sin(0.5k_y) \\
 H_0(2, 5) = H_0(4, 7) &= 2i * t_2 \sin(0.5k_x) & H_0(2, 6) = H_0(4, 8) &= -2i * t_2 \sin(0.5k_x) \\
 & & H_0(4, 9) &= -t_3 \\
 & & H_0(5, 6) = H_0(7, 8) &= -4 * t_4 \sin(0.5k_x) \sin(0.5k_y) \\
 H_0(5, 9) &= -2i * t_5 \sin(0.5k_x) & H_0(6, 9) &= -2i * t_5 \sin(0.5k_y) \\
 H_0(7, 9) &= 2i * t_5 \sin(0.5k_x) & H_0(8, 9) &= 2i * t_5 \sin(0.5k_y) \\
 & & H(4, 11) &= -t_6 \\
 H_0(5, 10) &= 2i * t_7 \sin(0.5k_x) & H_0(6, 10) &= 2i * t_7 \sin(0.5k_y) \\
 H_0(7, 11) &= -2i * t_7 \sin(0.5k_x) & H_0(8, 11) &= -2i * t_7 \sin(0.5k_y)
 \end{aligned} \tag{S4}$$

where $t_1 = -1.56, t_2 = 0.75, t_3 = -1.63, t_4 = 0.58, t_5 = 0.49, t_6 = 1.37, t_7 = 0.43$. The $H_0(\beta, \alpha)$ can be obtained

$$\begin{aligned}
 H_0(1, 1) = H_0(3, 3) &= -1.06 & H_0(2, 2) = H_0(4, 4) &= -1.16 \\
 H_0(5, 5) = H_0(6, 6) = H_0(7, 7) = H_0(8, 8) &= -4.94 \\
 H_0(9, 9) &= -4.30 & H_0(10, 10) = H_0(11, 11) &= -3.77
 \end{aligned} \tag{S5}$$

The Fermi surface of our Hamiltonian H_0 described above can be find in Fig. S6, which reproduces the Fermi surface found in DFT computations [3] on $\text{La}_3\text{Ni}_2\text{O}_7$ under high pressures.

For the interaction part of the 11-band Hubbard model, the Hund's coupling is adopted following Ref. [48], namely, we take into account the longitudinal component and neglect the transverse components of the Hund's couplings. It has been shown that this approximation affect the Mott physics only in a very minor way, as compared to the more rigorous "Kanamori" Hund' coupling [? ?].

close to 2, different DC schemes in fact give similar E_{dc} , hence lead to similar result. For example, at $\mu = 0$, using the Held's E_{dc} we get $n_h \approx 1.24, n_h^{IP} \approx 1.43, n_h^{OP} \approx 1.05$, while the fully localized or atomic limit (FLL) E_{dc} gives $n_h \approx 1.21, n_h^{IP} \approx 1.40, n_h^{OP} = 1.02$. We have also carefully checked that the DC term we use does not significantly shift the non-interacting Fermi surface.

The eleven-band Hubbard model

The tight-binding Hamiltonian H_0 of our 11-band Hubbard model is obtained from the Wannier downfolding of the DFT band structure as done in Ref. [3]. The values of the hopping amplitude and site-energies of H_0 are explicitly shown in the main text. The non-zero hoppings between $\alpha-, \beta-$ orbitals [$H_0(\alpha, \beta)$] can be listed as below (for $\alpha < \beta$),

as the hermitian conjugate of $H_0(\alpha, \beta)$. The site-energies read,

In Table-I in the main text, we have seen that even fully suppressing the Hund's coupling J_H , the result on the distribution of the holes does not significantly change.

Below we present a figure showing the local density of state (DOS) at $U = 9, U' = 6.3, J_H = 0, n_h = 1.05, T = 0.1$, from which we can see that the Zhang-Rice singlet band and charge-transfer characteristics are essentially the same as what we observed in the Fig.4 in the main text at $U = 7, U' = 5.6, J_H = 0.7, n_h = 1.045, T = 0.08$.

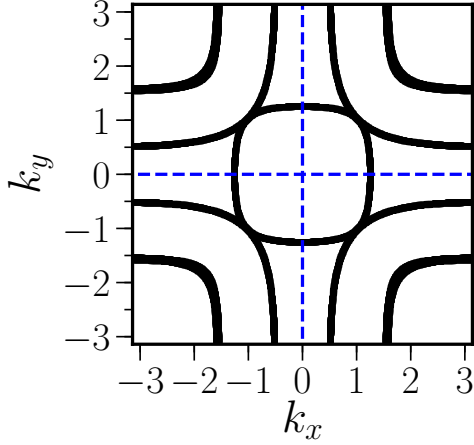


FIG. S6. Fermi surface of our 11-band tight-binding model.

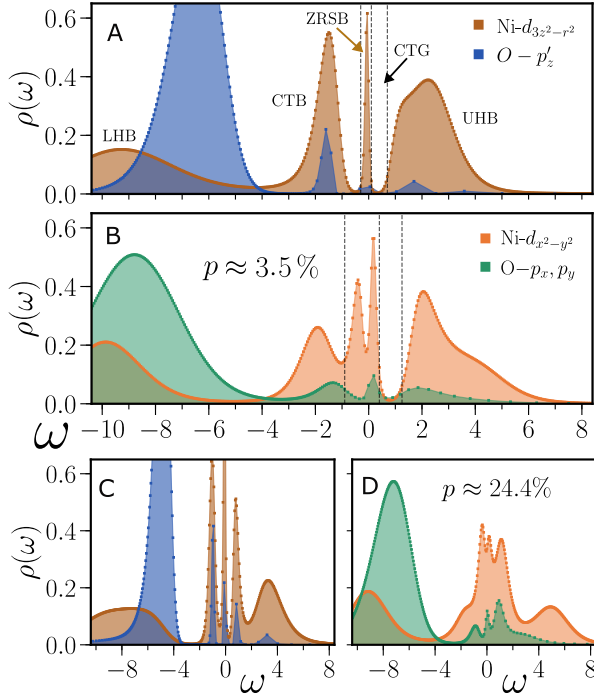


FIG. S7. Local density of states of the 11-band Hubbard model of a few Ni- d and O- p orbitals. Here $U = 9, U' = 6.3, J_H = 0, n_h = 1.05, T = 0.1$. See also Fig.4 of the main text.

Benchmarking the DQMC

In Fig. S8 we see that for the DQMC simulation at $T = 0.3$, changing system size from $6 \times 6 \times 11$ orbitals to $4 \times 4 \times 11$ orbitals does not essentially modify our result. Hence, the finite size effects in our study at these parameters are

negligible. In Fig. S9, comparison between the CDMFT and DQMC result on n_h are shown at temperature $T =$

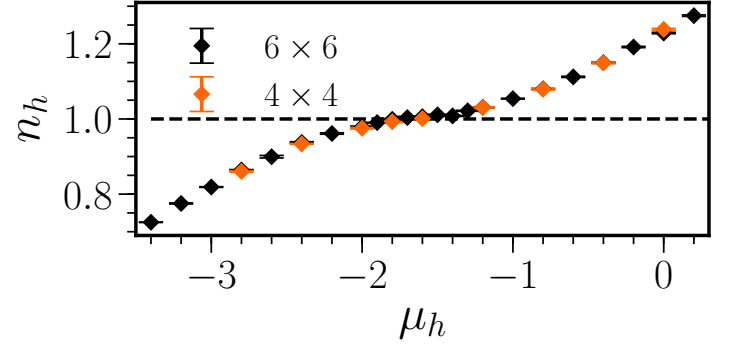


FIG. S8. Hole concentration as a function of hole chemical potential. Results are from two different lattice with periodic boundary conditions: $6 \times 6 \times 11$ -orbital and $4 \times 4 \times 11$ -orbital square lattices. Here $U = 7, U' = 5.6, J_H = 0.7, T = 0.3$.

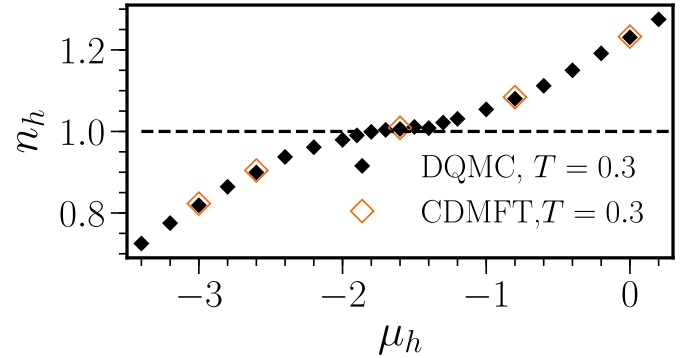


FIG. S9. Comparing the CDMFT and DQMC result on the Hole concentration as a function of hole chemical potential. Here $U = 7, U' = 5.6, J_H = 0.7, T = 0.3$.

0.3, where good agreement is seen in a wide chemical potential range.

Value of superexchange coupling J_1 between vertical $d_{3z^2-r^2}$ orbitals

By diagonalizing the 5-orbital O- p_z - Ni- $d_{3z^2-r^2}$ subsystem as shown in Fig. 1D, we find that the spin-singlet ground state has an energy gain $\tilde{J}_1 \sim -0.18eV$ over the spin-triplet states at $U = 7eV$. This value can be taken as a crude estimation of the Heisenberg exchange coupling J_1 between the vertical $d_{3z^2-r^2}$ electrons. The value of J_1 changes with U , as shown in Table. S2

U	E_0	E_1	$\tilde{J}_1 = E_0 - E_1$
6	-35.508	-35.293	-0.215
7	-36.697	-36.519	-0.178
8	-37.901	-37.751	-0.150
9	39.116	-38.988	-0.128

TABLE S2. Ground state energy E_0 and first excited state energy E_1 of the 5-orbital Hubbard model. Here $\mu = 0$, $E_{DC} = 2n_{d_{z^2}}^0 - 0.5 \approx 0.65U$.